Journal of Alloys and Compounds 509 (2011) 2856–2863

Contents lists available at ScienceDirect

Journal of Alloys and Compounds

journal homepage: www.elsevier.com/locate/jallcom

Excellent room-temperature ductility and formability of rolled Mg–Gd–Zn alloy sheets

D. Wu[a,b], R.S. Chen[a,*], E.H. Han[a]

[a] State Key Laboratory for Corrosion and Protections, Institute of Metal Research, Chinese Academy of Sciences, 62 Wencui Road, Shenyang 110016, China
[b] Graduate University of Chinese Academy of Sciences, Beijing 100049, China

ARTICLE INFO

Article history:
Received 8 August 2010
Received in revised form
22 November 2010
Accepted 23 November 2010
Available online 1 December 2010

Keywords:
Magnesium alloys
Rolled sheet
Non-basal texture
Ductility
Formability

ABSTRACT

In order to develop new magnesium alloy sheets with high formability at room temperature, the microstructure, texture, ductility, and stretch formability of rolled Mg–2%Gd–1%Zn and Mg–3%Gd–1%Zn sheets were investigated. The microstructures of these rolled sheets consist of fine recrystallized grains with a large amount of homogeneously distributed tiny particles in the matrix. The basal plane texture intensity is quite low and the basal pole is tilted by about 30° from the normal direction toward both the rolling direction and the transverse direction. The sheets exhibit an excellent ultimate elongation of ~50% and a uniform elongation greater than 30%, and the Erichsen values reach ~8 at room temperature. The flow curves of the two Mg–Gd–Zn alloys sheets display a remarkable linear hardening after an obvious yield point. The majority of the grains in the tilted texture have an orientation favorable for both basal slip and tensile twinning because of a high Schmid factor. The excellent stretch formability at room temperature can be attributed to the non-basal texture and low texture intensity, which led to the following characteristics: a lower 0.2% proof stress, a larger uniform elongation, a smaller Lankford value and a larger strain hardening exponent.

1. Introduction

Mg alloys have high potential for improving the fuel efficiency and reducing the CO_2 emission of vehicles because of their high specific strength and stiffness. There is an increasing demand for mass produced Mg alloy sheets with high performance for industrial applications. Unfortunately, the commercial magnesium alloys, e.g. AZ31 sheet, produced by the conventional rolling process usually have poor ductility and strong anisotropy at room temperature due to a pronounced basal texture [1], which limits their further press formability and industrial applications. Therefore, improving the low and/or room temperatures formability by changing or weakening the basal texture is important for promoting a wider use of Mg alloy sheets in industry.

Many different technologies, e.g. equal channel angular extrusion [2,3], differential speed rolling [4,5], torsion extrusion [6] and cyclic extrusion [7], have been used for processing magnesium alloys and have been proved to be effective in developing weaker or non-basal textures. The elongation-to-failure at room temperature can be enhanced significantly to ~38% [7]. However, these processing technologies are not as efficient as rolling process in view of industrial application.

Recently, the addition of rare-earth metal, such as Ce [8,9], Nd [9], Y [9,10] and Gd [11], to Mg alloy has been found to be an effective way of weakening and changing the basal texture of wrought magnesium alloys. Some work [8,9] attributes the texture weakening effect to the solute RE in Mg, and suggests that the addition of more RE should not be necessary for weakening the basal texture [11–13]; moreover, the excellent room temperature ductility and formability have indeed been observed in the Mg alloys with dilute (≤1 wt.%) RE elements [14–16]; the elongation-to-failure [16] and Erichsen value (IE) [14,15] at room temperature in those work are more than 30% and 9, respectively. However, in some other work [11,17,18], where RE is also present as a microalloying additions (≤1 wt.%), the room temperature ductility and formability are only enhanced moderately, still far inferior to typical structural Al alloys. So, it is still not sure that microalloying Mg with RE could promise excellent sheet formability. In fact, the effect of RE elements on weakening the texture and improving the ductility and formability of Mg alloy depends not only on the content, but also obviously on the type of RE addition [12] and other alloying elements in Mg [11,16,19], which has been scarcely discussed in those references.

Gd is soluble in magnesium to ~4 wt.% at 200 °C [20]. With Zn/Gd ratio in a certain range, there form a large amount of second-phase particles [21] in Mg matrix, which may serves as the sites of recrystallization, i.e. particle-stimulated nucleation (PSN), to weaken the texture [22]. Therefore, in Mg–Zn alloy, a relative high content of Gd, compared with dilute Gd addition [11,12,16], may act more

* Corresponding author. Tel.: +86 24 23926646; fax: +86 24 23894149.
E-mail address: rschen@imr.ac.cn (R.S. Chen).

0925-8388/$ – see front matter.
doi:10.1016/j.jallcom.2010.11.141

Table 1
Analyzed chemical compositions of the investigated alloys (wt.%).

Alloys	Gd	Zn	Mg
GZ21	1.68	1.11	Bal.
GZ31	2.74	1.06	Bal.

effectively on weakening and changing the basal texture in Mg sheet, and benefit its ductility and formability at room temperature more. In this paper, we add Gd as a major alloying element (the content of Gd higher than Zn) in Mg–Zn alloy and study the texture, ductility, strain-hardening behavior, and stretch formability of two rolled Mg–Gd–Zn alloy sheets with 2% and 3% Gd at room temperature. High room-temperature ductility and easy formability in these alloy sheets will be presented.

2. Experimental procedures

Two magnesium alloys denoted as GZ21 and GZ31 were examined in the present study. The chemical compositions are listed in Table 1. They were prepared with pure Mg (99.9%), Zn (99.9%) and Gd (99.5%) by melting under the protection of a mixed SF_6 (1, vol.%) and CO_2 (99, vol.%) atmosphere. Ingots with a dimension of 75 mm × 200 mm × 200 mm were prepared by pouring the melt into a preheated steel mold. They were homogenized at 500 °C for 10 h, then quenched in water, and subsequently machined to slabs with a dimension of 200 mm × 70 mm × 20 mm. The slabs were rolled to sheets at 430 °C with a final thickness of 3 mm. The rolling process started with an initial reduction of ~10% and the final reduction was ~30% resulting in a total reduction of 85%. After each pass, the rolling specimens were reheated to 430 °C and held for 20 min to maintain a consistent rolling temperature. The rolled sheets were annealed at 400 °C for 1 h after the last rolling pass. For comparison, AZ31 (Mg–3Al–1Zn–0.2Mn, by wt.%) was selected as the counterpart since it was a popular magnesium alloy for rolled sheets products. The cast ingot of the AZ31 magnesium alloy was machined to a slab with a thickness of 20 mm, and was also processed identically to the rolled Mg–Gd–Zn alloys. Hereafter, RD, TD and ND denote the rolling, transverse and normal directions of the sheets, respectively.

For microstructure observations, samples were cut from the rolled sheets and etched in acetic picric (25 ml ethanol + 2 g picric acid + 5 ml acetic acid + 5 ml water). The grain sizes (l) were determined by analyzing the optical micrographs with a line-intercept method ($d = 1.74l$). The phases were analyzed with a scanning electron microscope (SEM, Philips XL30 ESEM-FEG/EDAX) equipped with an energy-dispersive X-ray (EDX) spectroscopy analysis system and identified by X-ray diffraction using a monochromatic Cu K_α radiation. Texture analysis of the rolled samples in RD–TD plane was performed using the Schultz reflection method by X-ray diffraction. Calculated pole figures were obtained with the DIFFRAC^{plus} TEXEVAl software, using the measured incomplete {0002}, {10−10} and {10−11} pole figures.

Tensile specimens with 10 mm in gauge length, 4 mm in gauge width and 2.5 mm in gauge thickness were machined from the rolled sheets. The tensile tests were carried out at the angles of 0° (RD), 45° and 90° (TD) between the tensile direction and the RD at room temperature with an initial strain rate of $1 \times 10^{-3}\ s^{-1}$. The true plastic strains along the plate width (ε_w), thickness (ε_t) and length directions (ε_l), respectively, were measured on the specimens deformed at a plastic strain of 8%. From these results the Lankford values (r-value) were calculated using the equation $r = \varepsilon_w/\varepsilon_t = -\varepsilon_w/(\varepsilon_l + \varepsilon_w)$. The value of the strain hardening exponent (n-value) is equal to the true strain at the beginning of necking, and therefore it can be obtained by the formula $n = \varepsilon_T = \ln(1 + \varepsilon_E)$, where ε_T and ε_E are the true strain and engineering strain at the beginning of necking, respectively [23]. The engineering strain at the beginning of necking corresponds to the point of the ultimate tensile strength (UTS).

Circular blanks with a diameter of 60 mm and a thickness of 1 mm was machined from the specimens of rolled GZ21 and GZ31 sheets. Erichsen tests using a hemispherical punch with a diameter of 20 mm were carried out at room temperature to investigate the stretch formability of the specimens, and the Erichsen value (IE), which was the punch stroke at fracture initiation, was measured. The punch speed and blank-holder force were 5 mm/min and 10 kN, respectively. Graphite grease was used as a lubricant during the punch process.

3. Results

3.1. Microstructure and texture

The microstructures of the rolled GZ21 and GZ31 alloys in the RD–TD plane are shown in Fig. 1. Both alloys have equiaxed grain structures with a few twins. The average grain sizes of the two alloys are 16 μm and 12 μm, respectively. Fig. 2 is the SEM images of

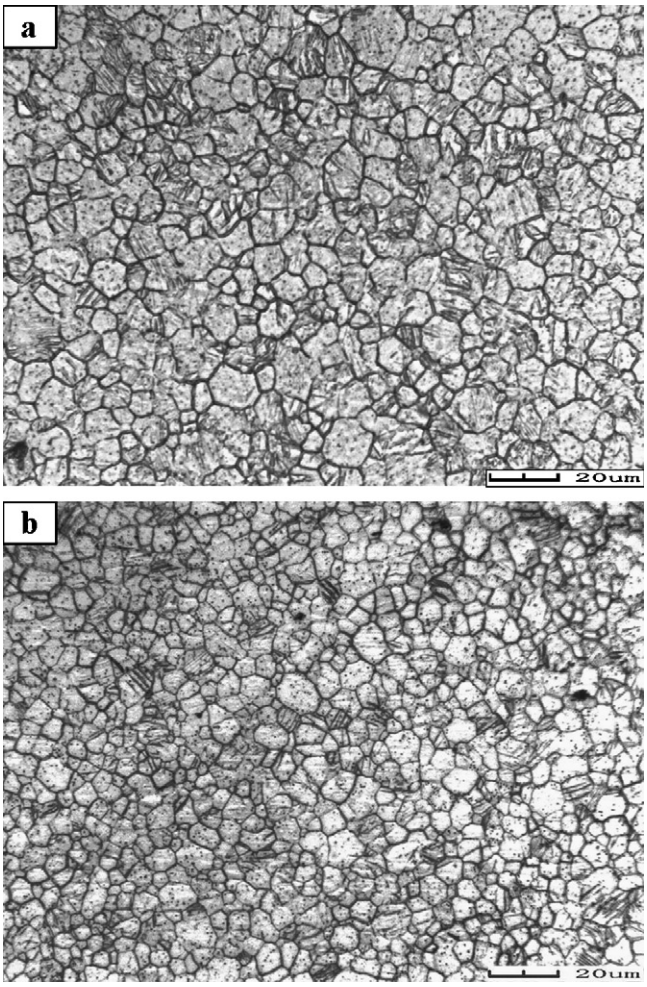

Fig. 1. Microstructures of the Mg–Gd–Zn sheets on RD–TD plane with RD parallel to scale bar: (a) GZ21 alloy and (b) GZ31 alloy.

the GZ31 sheet and corresponding EDX analysis results. In the SEM images, there are many fine particles smaller than 2 μm and some larger particles ~10 μm (Fig. 2a), which are homogeneously distributed in the matrix. A similar phase distribution is also observed in the GZ21 sheet. Studies by Yong Liu et al. have shown that alloys with the Zn/Gd ratio (at.%) in the range of 0.25–1 consist of α-Mg, w-phase and an unknown phase [21], and the w-phase is a MgZnGd compound with the fcc structure. The phase compositions of the present GZ21 (Zn/Gd = 1.2, at.%) and GZ31 (Zn/Gd = 0.8, at.%) sheets by XRD analysis are shown in Fig. 3. It indicates that the hot-rolled GZ21 and GZ31 alloys mainly consist of α-Mg solid solution, $Mg_3Gd_2Zn_3$ (w-phase) and $GdMg_5$ compounds. The larger particles are identified as $GdMg_5$ according to results of the EDX analysis, as indicated by arrows A and B in Fig. 2a.

The (0002) plane pole figures of the rolled Mg–Gd–Zn and AZ31 alloys sheets are summarized in Fig. 4 and reveal that the (0002) plane texture intensity of the Mg–Gd–Zn alloys sheets are far lower than that of the rolled AZ31. The maximum intensity (~2) of the Mg–Gd–Zn sheets is only a quarter of that of AZ31 sheet, which indicates that the addition of Gd effectively weaken the basal texture intensity. The same trend has been observed in other Mg alloys containing RE elements [9,18], but the effects in those cases were not as significant as in present Mg–Gd–Zn alloys. Meanwhile, the pole figures of GZ21 and GZ31 alloys sheets show a non-basal texture with basal poles tilting about 30° from the normal direction toward RD and TD, similar to that reported in [13,15]. And the peak intensity tilting toward TD is a little higher than that tilting to RD.

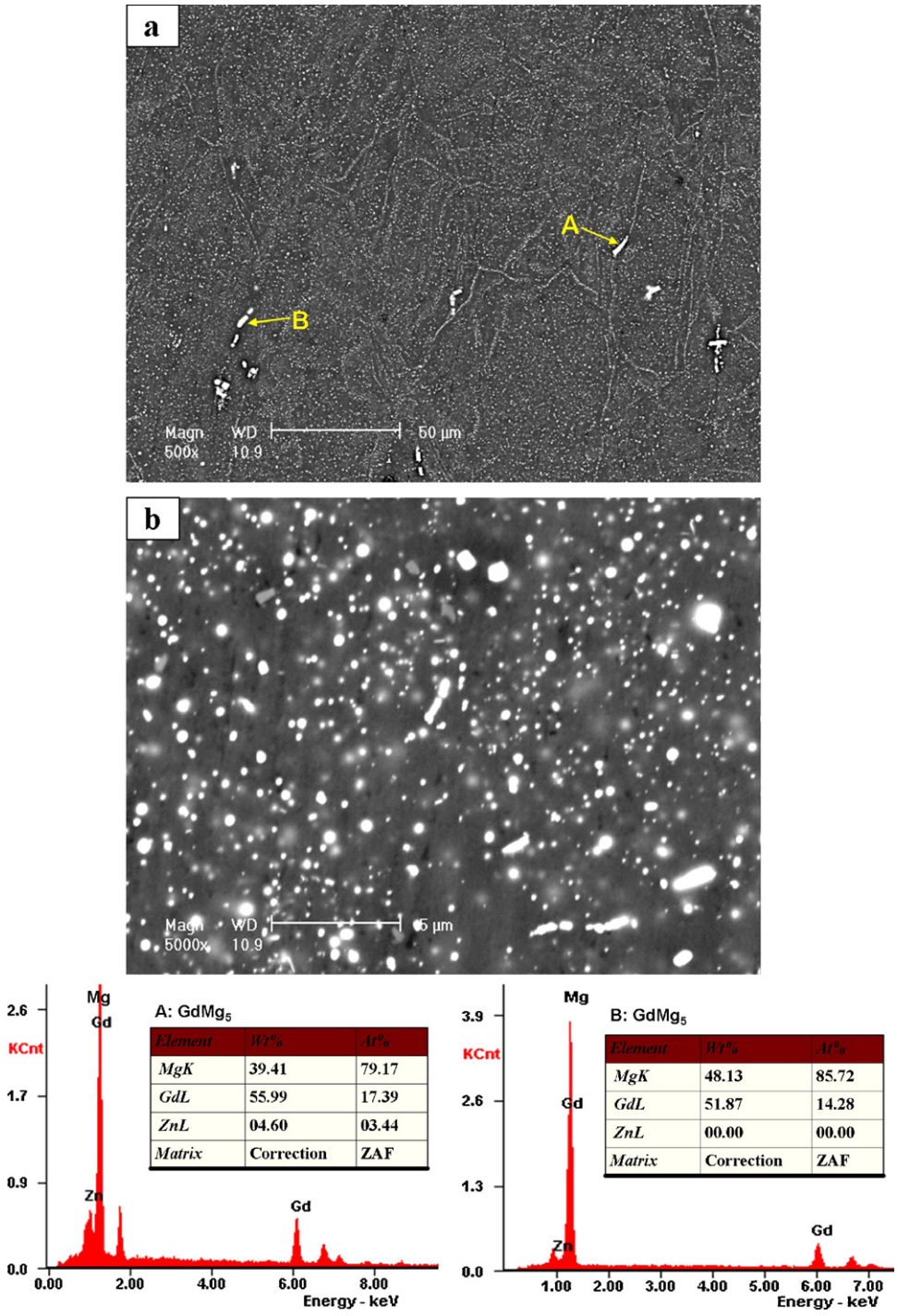

Fig. 2. SEM images (a and b) of the GZ31 sheet and corresponding energy dispersive X-ray spectra of points A and B indicated in the image (a).

The AZ31 sheet, on the other hand, shows a typical basal texture. In addition, the orientation distribution is wider in TD than in RD in the present Mg–Gd–Zn alloys sheets, while it is usually wider in RD in hot-rolled AZ31 sheet [5].

3.2. Mechanical properties and formability

Fig. 5 displays the typical engineering stress-engineering strain curves of the Mg–Gd–Zn sheets in the tensile directions of RD, 45° and TD. A distinct yield point can be found in the tensile curves except along RD of GZ21 (Fig. 1a), followed by strain hardening up to a peak stress. To compare with the data reported by other authors, we still define the tensile yield strength (TYS) of Mg–Gd–Zn alloys as the stress at an engineering strain of 0.2%. Both alloys exhibit planar anisotropy in the yield strength and elongation-to-failure, while the ultimate tensile strength (UTS) is not significantly affected by the sample orientation. The TYS in the RD of Mg–Gd–Zn alloys is higher than that measured at 45° and in the TD, while the elongation-to-failure is reverse. The average values for TYS, UTS and elongation-to-failure are summarized in Table 2. The elongation-to-failure of the Mg–Gd–Zn sheets exceeds 40%; the maximum elongation-to-failure of 47% is achieved along TD of GZ31 alloy, while that of the AZ31 alloy with a grain size of 12 μm is no more than 23% [4].

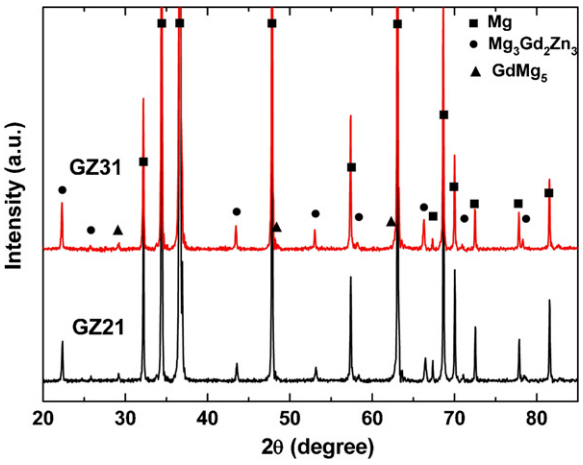

Fig. 3. X-ray diffraction patterns of the Mg–Gd–Zn sheets.

The strain hardening behavior of the Mg–Gd–Zn alloy sheets was analyzed by calculation of the strain hardening rate:

$$\theta \equiv \frac{d\sigma}{d\varepsilon} \tag{3}$$

where σ and ε are the true stress and true plastic strain, respectively, and the θ–σ curve for the Mg–Gd–Zn alloys sheets are shown in Fig. 6. Samples of the rolled sheets show first a steep hardening decrease due to a short elastoplastic transition, and further an almost constant hardening behavior, with $\theta \approx 1000$ MPa for GZ21 and 800 MPa for GZ31, which is linear hardening, and has great impact on ductility at room temperature, especially uniform elongation. We will discuss it in detail later.

It is known that the press formability of sheets at room temperature is strongly affected by the Lankford value (r-value). The r-values for Mg–Gd–Zn alloys sheets were investigated by conducting tensile tests and the results are summarized in Table 3, where the data of the rolled AZ31 sheets are also listed for comparison [24]. The average r-value ($\bar{r}$) and the planar anisotropy of the r-value (Δr) are expressed as [18]

$$\bar{r} = \frac{1}{4}\left|r_{RD} + r_{TD} + 2r_{45}\right| \tag{1}$$

$$\Delta r = \frac{1}{2}\left|r_{RD} + r_{TD} - 2r_{45}\right| \tag{2}$$

The average r-values of the Mg–Gd–Zn alloys ($\bar{r} = \sim 0.8$) are much lower than that of the rolled AZ31 sheets [24]. The low r-value less than unity indicate that sheet thinning can easily occur during in-plane tensile deformation. Moreover, the r-value of rolled

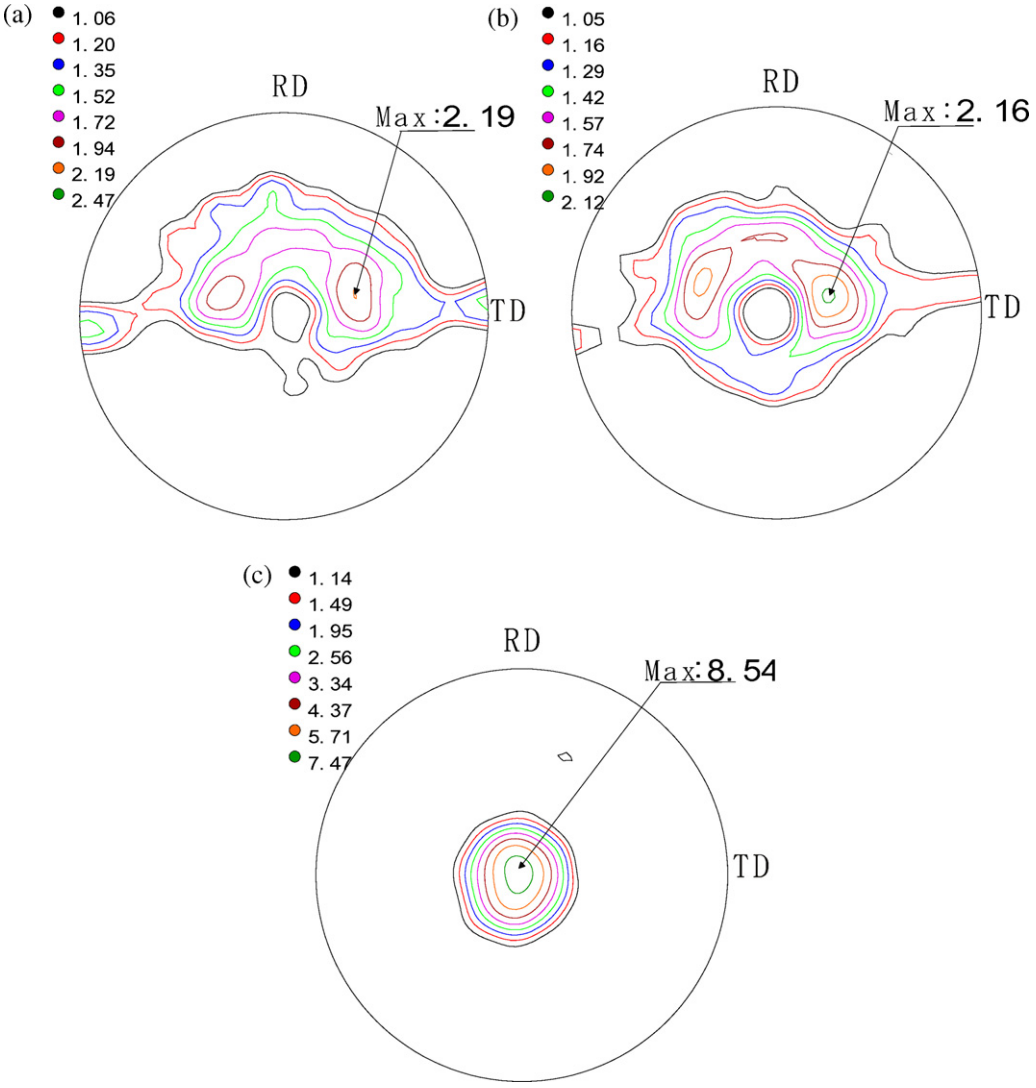

Fig. 4. (0002) pole figures of the rolled Mg–Gd–Zn alloys: (a) GZ21 alloy, (b) GZ31 alloy and (c) AZ31 alloy.

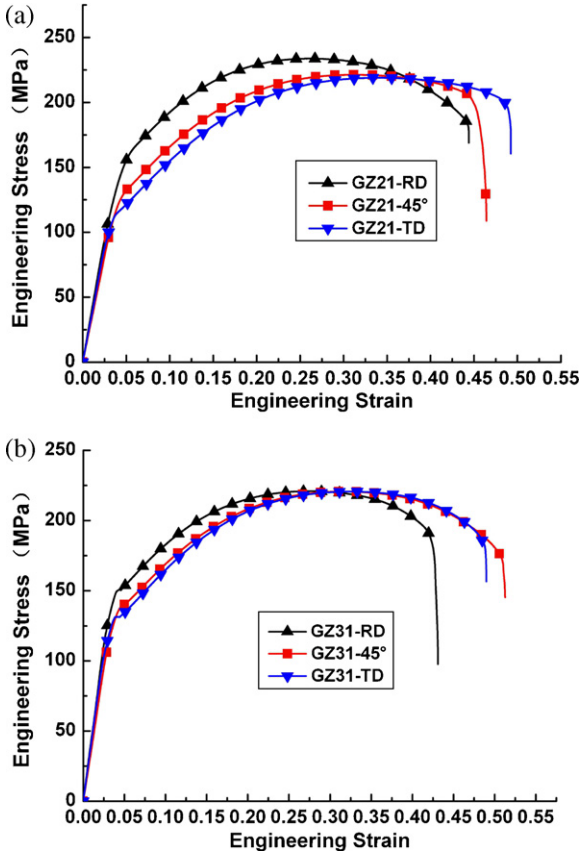

Fig. 5. Engineering stress-strain curves of the Mg–Gd–Zn sheets in the tensile directions of RD, 45° to RD and TD: (a) GZ21 and (b) GZ31.

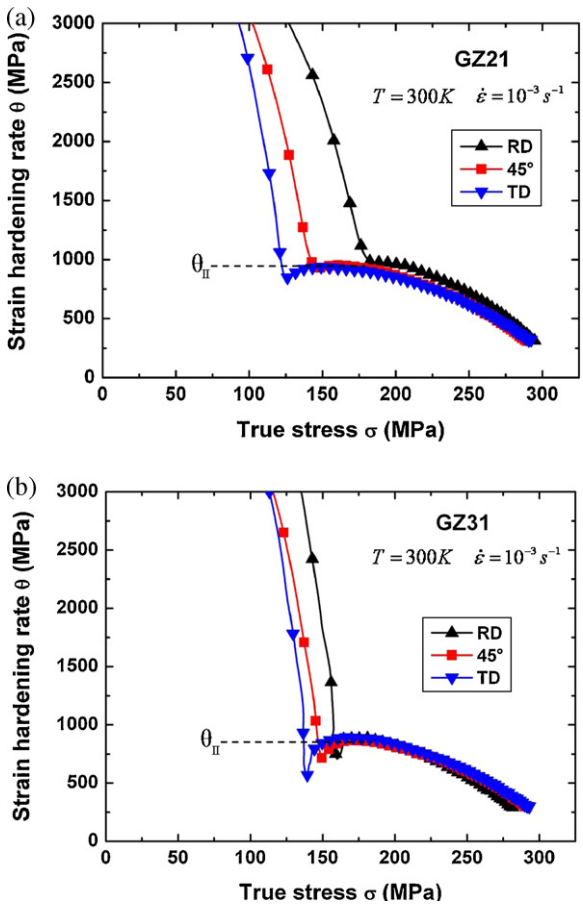

Fig. 6. Strain hardening behavior of the rolled Mg–Gd–Zn alloys: (a) GZ21 and (b) GZ31.

AZ31 sheets along different directions varied greatly, which would restrict the stretching capability [24]. In contrast, the *r*-values of the Mg–Gd–Zn sheets along different directions are close to 1. It is well known that the earring behavior of metal sheets during deep drawing is directly related to the planar anisotropy (Δr): sheets with low Δr exhibit less earring tendency. The Δr -value for the Mg–Gd–Zn sheets is close 0, which implies less earring possibility.

The results of the Erichsen tests at room temperature are shown in Fig. 7. The Erichsen values of GZ31 alloy were a little larger than that of GZ21 alloy, which is consistent with the ductile results of uniaxial tensile test. However, the Erichsen values are only 2.6 and 4.1 at room temperature and 433 K for normally rolled AZ31 Mg alloy sheets with a grain size of 16 μm [25], and the Erichsen values at room temperature are also only ~4.0 for the Mg–Ce alloy and differential speed rolling processed AZ31 Mg alloy sheets with a modified and weakened basal texture [17,25]. Comparatively speaking, the Mg–Gd–Zn alloys exhibited excellent stretch formability (IE ~8), which is a match for that of 5000 and 6000 series Al alloy, of which are about 9–10 [26,27] and much better than that of AZ31 Mg alloy sheets.

Fig. 7(c) and (d) are the top view of the rolled Mg–Gd–Zn alloys after the Erichsen tests. Previous study [28] revealed that a rolled AZ31 Mg alloy having a basal texture with a splitting of basal pole toward the RD exhibits a surface crack parallel to the RD after Erichsen tests. However, in the present study, the surface crack parallel to the TD appeared in all the rolled Mg–Gd–Zn alloys. The same phenomenon also appeared in the rolled Mg–Zn–Y alloys [15]. These results indicate that the splitting of basal pole toward the TD strongly affected the macroscopic fracture behaviors of the rolled Mg–Zn–RE sheet during Erichsen tests.

Table 2
Room-temperature tensile properties of the sheets (TYS, tensile yield stress; UTS, ultimate tensile stress).

Alloy	Grain size (μm)	Orientation	TYS (MPa)	UTS (MPa)	Elongation-to-failure (%)
GZ21	16	RD	129.9	233.4	40.3
		45°	113.8	221.2	44.5
		TD	110.1	218.4	44.6
GZ31	12	RD	130.6	220.0	40.3
		45°	121.0	220.3	47.3
		TD	118.0	220.9	45.1
AZ31 [4]	8	RD	185	259	23
		45°	188	262	23
		TD	201	262	21

4. Discussion

4.1. Texture

It is known that the basal plane of rolled AZ31 alloy sheet is intensively distributed parallel to the RD–TD plane, which cor-

Table 3
Planar and in-plane anisotropy of the Mg–Gd–Zn sheets.

Alloy	r_{RD}	$r_{45°}$	r_{TD}	$\bar{r}$	Δr
GZ21	0.8	0.6	0.8	0.75	0.2
GZ31	0.8	1	0.6	0.8	0.3
AZ31 [24]	2.2	3	4	3.1	

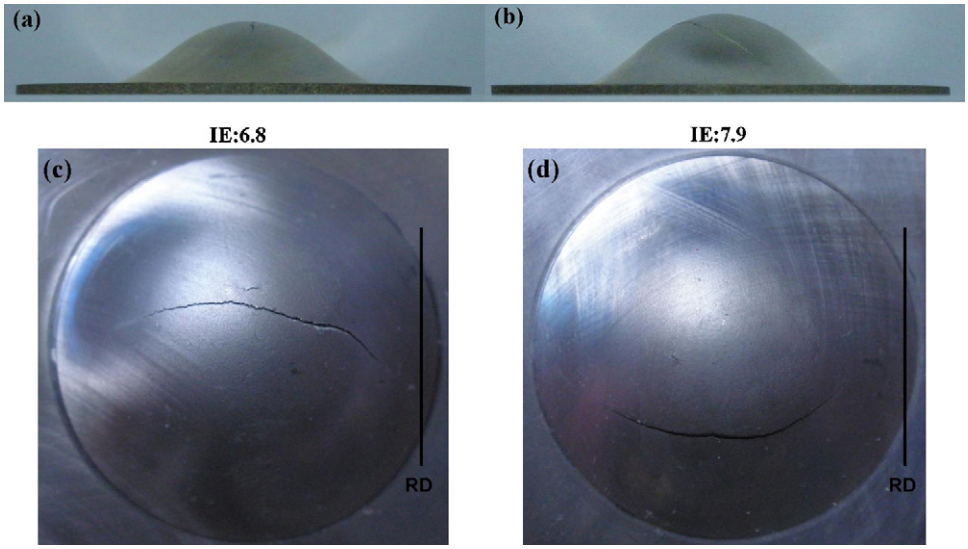

Fig. 7. Specimens and top view of the rolled Mg–Gd–Zn alloys after the Erichsen tests at room temperature: (a and c) GZ21 and (b and d) GZ31.

responds to a so-called basal-type texture. The other important feature of the AZ31 sheet texture is a broader intensity spread of the basal poles from the ND toward the RD than to the TD [5]. This type of texture has often been referred to as the typical texture of rolled or rather tempered Mg alloy sheets [1,5,29]. Some researchers have found that a combination of basal <a> slip and tensile twinning was responsible for the formation of strong basal texture in rolled AZ31 [29]. Furthermore, it has been emphasized that pyramidal <c + a> slip is responsible for the basal pole splitting toward the rolling direction. Interestingly, the (0 0 0 2) pole figure of the present Mg–Gd–Zn sheets exhibits an ellipsoidal form of the intensity distribution. The splitting angle of the basal pole from the ND toward the RD is about 30°, which is larger than AZ31 sheet. Furthermore, rotation of the basal poles by about 30° toward the TD is observed, which does not occur in AZ31. This unusual type of texture developed during sheet rolling has been noted by many other authors [13–17,30,31], who further suggested that additions of RE elements to Mg alloys should be responsible for the development of weaker textures during rolling or extrusion [14,18]; however, a number of different mechanisms for this texture has been suggested. One of the possible origins of the splitting of basal pole toward the TD is an activation of prismatic <a> slips. Lebensohn et al. [32] have simulated basal texture changes during hot rolling of a Zr alloy with hcp structure, and demonstrated that the development of splitting of basal pole toward the TD is caused by an activation of prismatic <a> slips. Indeed, previous study [17] has revealed that RE (Ce) addition in Mg activates prismatic <a> slips. The above information suggests that the splitting of basal pole toward the TD may be related to the activation of prismatic <a> slips due to Gd addition. A RD–TD double split was also observed in Mg–Zn–Ce alloy [13]. The author attributed the particular texture to that the non-basal orientations develop a form of growth advantage, and grow at the expense of the basal grains, possibly due to the a form of particle pinning or solute drag that alters orientation relationships for high boundary mobility. In addition, particle stimulated nucleation (PSN) of recrystallization has also been cited as a texture-randomizing mechanism in wrought magnesium alloys [22]. The alloys investigated in this study contain fine particles, i.e. w-phase. Thus, the random texture in the Gd-containing Mg alloys may have originated from the special recrystallization behaviors during the rolling process. In fact, a lot of annealing treatments to the rolled GZ31 sheet have be conducted, and we found the fine w-phase in matrix greatly influences the type and intensity of the texture after annealing treatment. Further work is underway to understand the relationship among fine w-phase in the matrix, recrystallization behavior and texture of Mg–Gd–Zn alloy sheets.

4.2. Ductility

The uniform elongation and post-uniform elongation are summarized in Fig. 8. As seen in Fig. 8(b), the post-uniform elongations of the Mg–Gd–Zn alloys sheets are almost the same as that of AZ31 alloy, which means the uniform deformation stage plays a vital role in achieving the high ductility of the rolled Mg–Gd–Zn sheets. The hardening capability of the processed materials confers the resistance to developing tensile mechanical instabilities, and therefore controlling ductility. Higher strain-hardening exponent (n value) usually indicates better ductility, especially uniform elongation at room temperature. For metal sheets with high ductility, such as Al or steel, n values are typically about 0.20–0.50 at room temperature [33], while the n values of most magnesium alloys are lower than 0.2. For example, n values of AZ31 and AM30 alloy sheets were 0.14 and 0.17, respectively [34]. However, the present Mg–Gd–Zn sheets exhibit high n values ranging from 0.24 to 0.29 as observed in this study (see Table 4).

Detailed studies on strain hardening behaviors of single crystals of pure magnesium were performed even before 1980 [35]. Three strain hardening stage in hexagonal metals are observed as in face-centered cubic (fcc) crystals [36], i.e. stages I–III, (1) an initial transient stage, where θ decreases rapidly (stage I), (2) a stage where θ increases to a maximum and then keeps nearly constant with σ (stage II) and (3) a stage where θ decreases linearly with σ due to onset of dynamic recovery (stage III). In the stage II of strain hardening, the strain hardening rate keeps nearly constant with stress increasing, therefore, stage II is linear hardening, which guarantees the tensile mechanical stabilities and high uniform elongation. However, the texture has a great influence on strain hardening of magnesium alloy polycrystals. del Valle et al. [37] reported that rolled samples with intensive basal texture show a suppression of stage II and a development of a linear stage III from the beginning of deformation by the enforcement of prismatic slip, resulting in a low elongation, when the tensile test is conducted along RD, while samples with ideal orientation of the basal planes (45° to tensile axis) processed by equal channel angular extrusion show extensive stage II of strain hardening, leading to a excellent ductility at room temperature. The present Mg–Gd–Zn alloy sheets

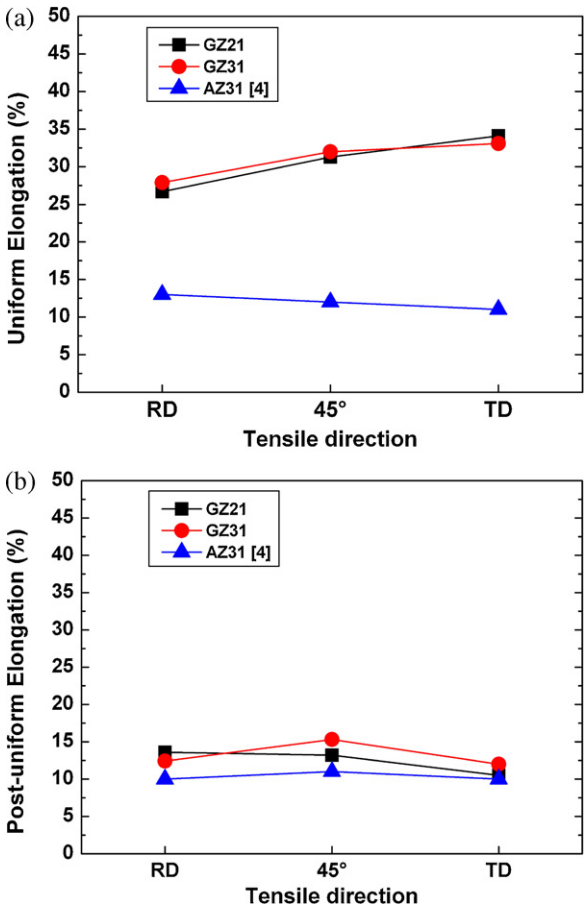

Fig. 8. (a) The uniform elongation and (b) post-uniform elongation and of GZ21, GZ31 and AZ31 sheets.

also exhibit a remarkable stage II of strain hardening when tensile tested at room temperature. And it is worth to note that the stage II of strain hardening appears without dependence on sample orientation; this can be attributed to the symmetrical splitting of the basal poles around the ND and the random texture of the rolled Mg–Gd–Zn alloys, and in turn the basal slip is favored in almost all direction in the RD–TD plane. However, the stage II of strain hardening of samples in TD is stabler than that of samples in RD. For instance, the stage II of GZ21 alloy in TD stay from $\sigma = 125$ MPa to 175 MPa, while the range of stage II of GZ21 alloy in RD is only about 20 MPa. We can ascribe this phenomenon to the higher peak intensity tilting toward to TD. In contrast to RD, TD is a more desirable orientation of the basal planes for tensile test. The stabler stage II of strain hardening interprets the higher elongation in TD. The quite random texture and the tilted basal pole from ND of rolled Mg–Gd–Zn alloys corresponds to a linear strain hardening behavior (the appearance of stage II of strain hardening) in tensile test, which brings about the high tensile ductility.

Table 4
Strain-hardening exponent of the Mg–Gd–Zn alloys along different directions.

Alloy	RD	45°	TD
GZ21	0.24	0.27	0.29
GZ31	0.25	0.28	0.29
Low carbon steel [33]	0.20–0.25		
Al alloy [33]	0.20–0.30		
AM30 [34]	0.17	–	–
Rolled AZ31 [34]	0.14	–	–

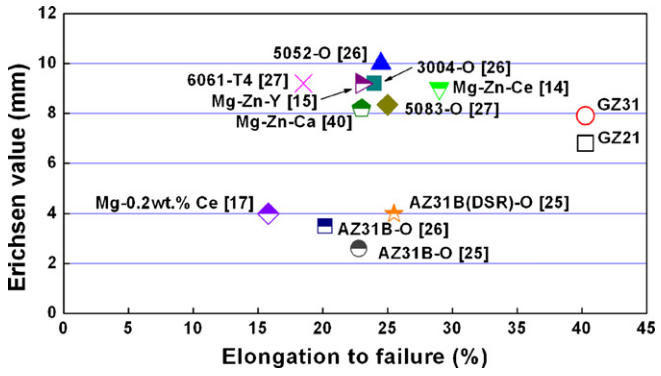

Fig. 9. Relationships between tensile elongation (elongation-to-failure) and stretch formability (Erichsen value) in the present alloys; the data for typical commercial Mg alloy and Al alloys are also included for comparison.

4.3. Formability

Rolled AZ31 sheets with strong basal texture were reported to exhibit a *r*-value as high as 3 [24] due to a small thickness-direction strain and/or a large width-direction strain. In contrast, the *r* values close to 1 in the rolled Mg–Gd–Zn alloys indicate that the cross-sectional contraction occurs isotropically, i.e. the strains in the width and thickness directions are similar. It is well know that the *r* values have a strong relationship with the texture. The rolled Mg–Gd–Zn alloys have a rather random texture and the basal pole tilts away from ND, and the majority of grains in the random and modified texture have an orientation favorable for basal slip during tensile tests, which produces a thickness-direction strain and a length-direction strain. As a result, the thickness-direction strain is comparable with width-direction strain and a moderate *r*-value of around 1 is obtained. The low *r*-value is said to be a characteristic of Mg alloys containing RE elements [18]. When the basal planes are aligned parallel to the tensile direction, the basal and prismatic <a> slips cannot play a vital role in the thickness-direction strain [15,24]. Also, the strong basal texture restricts the activation of $\{1\,0\,-1\,2\}$ twinning because $\{1\,0\,-1\,2\}$ twinning occurs under tension parallel to the *c*-axis or under compression perpendicular to the *c*-axis. Therefore, it is suggested that the lower average *r*-value and its lower anisotropy for the Mg–Gd–Zn alloy sheets should be attributed to the quite low texture intensity and the splitting of the basal plane.

Sheet metal forming processes can be characterized by two basic types of deformation patterns: drawing and bending. Concerning drawing one has to distinguish stretching ($\varepsilon_1 > 0$, $\varepsilon_2 > 0$) and deep drawing ($\varepsilon_1 > 0$, $\varepsilon_2 < 0$) [38]. In our paper, Erichsen tests were carried out at room temperature to investigate the stretch formability of the Mg–Gd–Zn sheets. During the Erichsen test, the sheet specimen continues thinning until the occurrence of fracture [39]. Thus, the lower *r*-value of the Mg–Gd–Zn alloy sheets, which means a good sheet shinning ability, is considered to contribute much to its excellent stretch formability.

The tensile elongation and stretch formability balance in the present Mg–Gd–Zn alloys is shown in Fig. 9, and the data for typical commercial Mg alloy and Al alloys are also included for comparison [14,15,17,25–27,40]. The present Mg–Gd–Zn alloys shows higher tensile elongation compared with traditional Mg alloy sheet. And its stretch formability is also much higher than that of AZ31 sheet, but very close to that of some Mg–Zn–RE alloy sheets [14,15]. It is interesting that the IE values of Mg–Gd–Zn alloys are a little lower than that of typical structural Al alloys, though the elongation of Mg–Gd–Zn alloys is obviously higher. In the case of a biaxial tensile stress state, the strain in the tensile direction and width direction are positive, while strain in the thickness is negative, which are

different from the stress state of uniaxial tensile test. Thus, the high elongation is only a necessary condition for excellent stretch formability, and the low anisotropy (low *r*-value) and high strain hardening capability (high *n*) seems to be more important.

5. Conclusions

The rolled Mg–Gd–Zn alloys with excellent ductility and formability at room temperature are developed, and the results are summarized as follows:

1. The rolled Mg–Gd–Zn alloys have fine recrystallized microstructures with a large amount of tiny particles homogeneously distributed in the matrix.
2. The Mg–Gd–Zn sheets have an oval-shaped distribution of basal poles at angles of about 30° to normal direction (ND) of the sheets, and it seems that the basal texture intensity is effectively weakened by the addition of Gd.
3. The distinct textures and low texture intensity of the sheets result in a linear hardening behavior, a high strain hardening exponent (*n*) and a low lankford value (*r*) in uniaxial tensile test at room temperature.
4. The sheets exhibit a large elongation-to-failure (nearly 50%), uniform elongation (larger than 30%) and a high Erichsen values (nearly 8) at room temperature, due to the excellent strain hardening capability, high *n* value and low *r* value.

Acknowledgements

This work was funded by the National Basic Research Program of China (973 Program) and National Natural Science Foundation of China (NSFC) through projects No. 2007CB613704 and No. 50874100, respectively.

References

[1] P. Chen, D. Shang, R. Xiao, G. Huang, Q. Liu, Trans. Nonferrous Met. Soc. China 20 (2010) s589–s593.
[2] W.M. Gana, M.Y. Zheng, H. Chang, X.J. Wang, X.G. Qiao, K. Wu, B. Schwebke, H.-G. Brokmeierb, J. Alloys Compd. 470 (2009) 256–262.
[3] L.B. Tong, M.Y. Zheng, X.S. Hu, K. Wu, S.W. Xu, S. Kamado, Y. Kojima, J. Alloys Compd. 527 (2010) 4250–4256.
[4] X. Huang, K. Suzuki, A. Watazu, I. Shigematsu, N. Saito, Mater. Sci. Eng. A 488 (2008) 214–220.
[5] J.B. Lee, T.J. Konno, H.G. Jeong, J. Alloys Compd. 499 (2010) 273–277.
[6] Y. Chino, K. Sassa, M. Mabuchi, Scr. Mater. 59 (2008) 399–402.
[7] J. Lin, Q. Wang, L. Peng, H.J. Roven, J. Alloys Compd. 476 (2009) 441–445.
[8] M. Masoumi, M. Hoseini, M. Pekguleryuz, Mater. Sci. Eng. A (submitted for publication).
[9] K. Hantzsche, J. Bohlen, J. Wendt, K.U. Kainer, S.B. Yi, D. Letzig, Scr. Mater. 63 (2010) 725–730.
[10] S. Sandlobes, S. Zaefferer, I. Schestakow, S. Yi, R. Gonzalez-Martinez, Acta Mater. 59 (2011) 429–439.
[11] N. Stanford, D. Atwell, M.R. Barnett, Acta Mater. 58 (2010) 6773–6783.
[12] N. Stanford, Mater. Sci. Eng. A 527 (2010) 2669–2677.
[13] L.W.F. Mackenzie, M.O. Pekguleryuz, Scr. Mater. 59 (2008) 665–668.
[14] Y. Chino, K. Sassa, M. Mabuchi, Mater. Trans. 49 (2008) 2916–2918.
[15] Y. Chino, K. Sassa, M. Mabuchi, Mater. Sci. Eng. A 513–514 (2009) 394–400.
[16] H. Yan, R.S. Chen, E.H. Han, Mater. Sci. Eng. A 527 (2010) 3317–3322.
[17] Y. Chino, M. Kado, M. Mabuchi, Mater. Sci. Eng. A 494 (2008) 343–349.
[18] J. Bohlen, M.R. Nurnberg, J.W. Senn, D. Letzig, S.R. Agnew, Acta Mater. 55 (2007) 2101–2112.
[19] H.K. Lim, D.H. Kim, J.Y. Lee, W.T. Kim, D.H. Kim, J. Alloys Compd. 468 (2009) 308–314.
[20] L.L. Rokhlin, Magnesium Alloys Containing Rare Earth Metals, Taylor & Francis, London, 2003.
[21] Y. Liu, G. Yuan, S. Zhang, X. Zhang, C. Lu, W. Ding, Mater. Trans. 45 (2008) 941–944.
[22] A. Sadeghi, M. Pekguleryuz, Mater. Sci. Eng. A (2010), doi:10.1016/j.msea.2010.10.096.
[23] J.H. Wang, J.P. Zheng, J.C. Liu, D.H. Hang, Mechanical Behavior of Materials, Tianjin University Press, Tianjin, 2006.
[24] Y. Chino, M. Mabuchi, Scr. Mater. 60 (2009) 447–450.
[25] X.S. Huang, K. Suzuki, A. Watazu, I. Shigematsu, N. Saito, J. Alloys Compd. 470 (2009) 263–268.
[26] Japan Light Metal Association (Ed.), Aluminum Handbook, Japan Light Metal Association, Tokyo, 2000, p. 98.
[27] M. Sugamata, J. Kaneko, M. Numa, J. Jpn. Soc. Technol. Plast. 41 (2000) 233–238.
[28] Y. Chino, K. Sassa, A. Kamiya, M. Mabuchi, Mater. Trans. 47 (2006) 2555–2560.
[29] A. Styczynski, C. Hartig, J. Bohlen, D. Letzig, Scr. Mater. 50 (2004) 943–947.
[30] D.H. Kang, D.W. Kim, S. Kim, G.T. Bae, K.H. Kim, N.J. Kim, Scr. Mater. 61 (2009) 768–771.
[31] K. Hantzsche, J. Wendt, K.U. Kainer, J. Bohlen, D. Letzig, JOM 69 (2009) 38–42.
[32] R.A. Lebensohn, M.I. González, C.N. Tomé, A.A. Pochettino, J. Nucl. Mater. 229 (1996) 57–64.
[33] O. Duygulu, S.R. Agnew, Magnes. Technol. (2003) 237–242.
[34] A.A. Luo, A.K. Sachdev, Metall. Mater. Trans. A 38A (2007) 1184–1192.
[35] P.B. Hirsch, J.S. Lally, Philos. Mag. 12 (1965) 595.
[36] E. Schmid, W. Boas, Kristallplastizitat, Springer Verlag, Berlin, 1935.
[37] J.A. del Valle, F. Carreno, O.A. Ruano, Acta Mater. 54 (2006) 4247–4259.
[38] D. Banabic, H.J. Bunge, K. Pohlandt, A.E. Tekkaya, Formability of Metallic Materials, Springer-Verlag, Berlin, 2000.
[39] A.M. Erichsen, Stahl und Eisen 34 (1914) 879–882.
[40] Y. Chino, X. Huang, K. Suzuki, M. Mabuchi, Mater. Trans. 51 (2010) 818–821.